ARTICLE

# Formation of Complexes between Nanoparticles and Weak Polyampholyte Chains. Monte Carlo Simulations

Serge Ulrich,*,[†] Marianne Seijo,[‡] Fabrice Carnal,[†] and Serge Stoll[†]

[†]F.-A. Forel Institute, Group of Environmental Physical Chemistry, University of Geneva, 10 Route de Suisse, 1290 Versoix, Switzerland

[‡]Laboratory of Computational Systems Biotechnology (LCSB), EPFL/SB/ISIC/LCSB, Station 6, CH-1015 Lausanne, Switzerland

ABSTRACT: The electrostatic driven complex formation between a weak polyampholyte chain and one positively charged nanoparticle is investigated using Monte Carlo simulations. The influence of parameters such as the polyampholyte contour length, number and size of blocks, nanoparticle surface charge density, and solution properties, such as the pH and ionic concentration, on the PA titration curves is investigated. It is shown that the presence of one positively charged nanoparticle significantly modifies the acid/base properties of the weak polyampholyte by, on the one hand, promoting the formation of negatively charged monomers and, on the other hand, limiting the number of positively charged monomers. The electrostatic interactions of this system can be modified by pH, ionic concentration, and nanoparticle surface charge. The competition between attractive and repulsive, intramolecular and intermolecular electrostatic interactions leads to a wide range of possible PA conformations at the nanoparticle surface, which have a direct impact on the nanoparticle stabilized or destabilized solutions. Extended conformations, electrostatic rosettes, and dense multiplayer structures are observed. Nonetheless, the intramolecular interactions between the positively and negatively charged PA monomers, in particular at the isoelectric point, are found to play important and subtle roles for both the isolated and adsorbed chain conformations. It is also found that nanoparticle charge inversion is an important ingredient for the formation of multilayer structures at the nanoparticle surface.
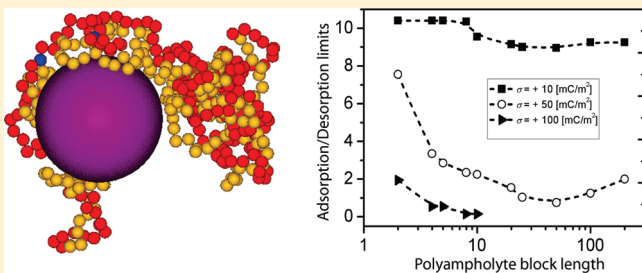
1. INTRODUCTION

Charged polymers, also known as polyelectrolytes (PEs), constitute a common and fascinating class of polymers owing to their importance in soft matter research, material sciences, bioactive nanoparticles, and molecular biology.[1−8] Electrostatic interactions between charged monomers lead to the rich behavior of polyelectrolyte solutions which are significantly different from those of uncharged polymers. Compared to neutral polymers, polyelectrolyte theory remains less developed. For instance, the conformational chain properties can be described with scaling laws in the case of neutral or hydrophobic polymers, whereas electrostatic interactions in polyelectrolytes introduce additional length scales and complexity.[9] The most prominent features of charged polymers are a high solubility in water or polar solvent and a strong adsorbing capacity at oppositely charged surfaces including charged polymers, layers, nanoparticles, micelles, dendrimers, and biomacromolecules. The design of multicomponent films by the successive deposition of anionic and cationic PEs is of main interested since the soft structure is dynamic, and the distance between the layers can be adjusted by controlling the degree of swelling.[10] The complexation of charged polymers with superparamagnetic nanoparticles allows to achieve a better contrast in magnetic resonance imaging than single

nanoparticles showing benefits of PEs for biomedical applications.[11]

Many natural PEs such as proteins and polysaccharides are in fact polyampholytes. Polyampholytes (PAs) are defined as polyelectrolyte chains composed of monomer units having ionizable groups of both positive and negative charges such as synthetic copolymers made of monomers with acidic and basic groups. Experimentally, the first studies of PAs were reported more than 50 years ago[12,13] discussing the chain isoelectric point determination using viscosity measurements. For several years, complexes formation between PA and PE chains also received a lot of attention due to their numerous applications in the everyday life.[3,14−18] For example, Leal Denis et al.[19] recently investigated the interactions between a synthesized PA and the BSA protein, and it was found that the amphoteric properties of the two PEs allow complex formation even if both the PA and protein have negative net charges.

The adsorption of PA chains on various charged surfaces also remains challenging since they are involved in many industrial coating, surface functionalization processes,[20] or in more unusual applications such as the preparation of gold nanoparticles using a

gold precursor and a reductive agent.[21] Parameters such as the ionic concentration or surface charge are playing key roles in the adsorption process, and it is usually found that by increasing the ionic strength, the adsorption process becomes more efficient due to the increased screening of the electrostatic repulsions.[22] By studying the loop size distributions of adsorbed PAs on a surface, Ozon et al.[23] found that the number of monomers in a loop decreases with a higher surface charge. Also, the PA adsorption was found stronger in the isoelectric domain due to polarization-induced attractive interactions.[22,24,25] Indeed, the net charge is zero on average, but locally positive or negative, hence leading to attractive electrostatic interactions between the different parts of the chain and surface. Even if the net charge of the PA is not neutral and bears charges of the same sign than the surface, complexation is observed. Adsorption processes between a PA and flat or curved surfaces were also addressed in a number of theoretical papers, where different models of adsorption were proposed as a function of specific surface charge density ranges and surface size.[26,27] In order to better understand the parameters influencing the adsorption mechanism, Netz and Joanny[28] provide theoretical phase diagrams for the adsorption of a PA chain on charged spheres. In a salt-free environment, it was found that a short PA chain adsorbs as a single coil which is stretched (pole regime). On the other hand, long PA chains may adsorb as a whole or may be dissolved and adsorbed in a coil-like state depending on the fraction of charged monomers and the sphere charge. The subtle competition between repulsive intramonomer interactions and attractive monomers−spherical surface interactions can also lead to a multilayer adsorption. It was found that by adding salt, the size of the adsorbed PA chain is limited to the screening length. Considering a planar surface, the adsorption/desorption limit disappears, leading to the complexation of infinitely long chains even for low surface charge and fraction of charged monomers. This single PA chain adsorption model was then extended to the case of multichain adsorption on charged spherical particles and planar surfaces.[29−31] To consider the effect of the heterogeneity of surfaces, de Vries and coworkers[32] developed an analytical theory for the interaction of PAs (and PEs) with proteins. This approach was addressed in terms of PAs (and PEs) adsorption on randomly charged surfaces. Below a critical salt concentration, the analytical estimates let appear an adsorption even if the net charges of chains and surfaces are the same, which is consistent with experimental investigations on arabic gum and whey protein isolate.[33]

Monte Carlo simulations have corroborated experimental and theoretical results concerning PAs adsorption with spherical particles and surfaces, but only a few papers were addressed. The influence of different parameters on complexation processes between particles and PAs such as the particle size, particle charge, and charged fraction of monomers was investigated by Feng and Ruckenstein.[34] In the case of a small particle, PA conformations such as spherical dumbbell, necklace, and rod were observed by decreasing the positive PA charge fraction. The particle size was also found an important parameter for large particles, where the surface becomes large enough to adsorb the whole amphoteric chain. Concerning a planar charged surface instead of a spherical particle, several groups[35,36] found results that confirm experimental and theoretical data; i.e., the PA adsorption occurs when the local attraction with the surface becomes stronger than the net charge repulsion. Consequently, short PA chains remain in bulk while chain entropy is stronger than chain polarizability, and the adsorption process increases with the PA length, PA block size, and surface charge.

Concerning PE−PA complexes, Jeon and Dobrynin[37] studied the effect of PA charge sequence on the final conformations by molecular dynamics simulations. Flower- and tadpole-like structures were observed with random and diblock PAs, respectively, demonstrating the importance of the PA primary structure on the complex formation. Since anionic PAs play an important role in gene transcription process, Yoshihara et al.[38] showed with the help of Monte Carlo simulations that the net dipole of anionic PAs separates oppositely charged DNA and polycation through electrostatic bridging, leading to the increase of the transcription rate.

Recently, more complicated systems comprising diblock polyampholytes grafted onto uncharged spherical particles were investigated by Monte Carlo simulations.[39−41] The brush structures as a function of the charge ratio and the stiffness of the two blocks were examined. Flexible PA chains were found to form a compact and disordered layer around the particle independently of the fractional charge per segment, and the increase of chain rigidity resulted in more ordered and less dense structures. At the highest linear charge density, blocks of opposite charge were strongly associated leading to PA star structures. In the case of several spherical particles, small clusters were observed when the charges of the two blocks were identical. Considering a flat surface instead of spherical particle, Baratlo and Fazli[42] observed by molecular dynamics simulations a linear dependence of the average brush thickness of flexible, semiflexible, and rodlike diblock PAs as a function of the grafting density, and it was found that a simple scaling method describes well this linear dependence in the case of flexible chains.

Monte Carlo simulations were also used to study in a systematic way the complexation of a weak PE with an oppositely charged nanoparticle (NP) by considering titration curves.[43,44] Several competing effects were pointed out such as the attractive interaction between the charged PE monomers and the NP or the increase of the electrostatic repulsions along the PE chain with the increase of the pH of the solution. Primary structure and stiffness of a weak PA chain were also concomitantly investigated.[45] It was found that primary structures play a key role onto the acid/base properties of rodlike PAs and clearly show a heterogeneous charging process along the rodlike PAs, i.e., charges accumulated preferentially at the chain or block extremities. On the other hand, flexibility allows the PAs to adopt dense conformation and hence to optimize ion pairing. The aim and originality of the present paper consist to study the complex formation between a weak polyampholyte chain and a positively charged nanoparticle by means of Monte Carlo simulations. Molecular parameters, block and chain lengths, nanoparticle surface charge density, and solution features, such as the pH solution and ionic concentration, are investigated to get an insight into their effects on the formation of PA and nanoparticle complexes and for a better understanding of the rational formulation, design, and stability of PA−nanoparticle complexes as well as, from a more perspective point of view, the question of protein recognition via charge complementarity with polyelectrolyte surfaces which has considerable value in biosensors and for protein separations.

2. MODEL DESCRIPTION

One linear polyampholyte is generated in a three-dimensional and off-lattice space. A coarse-grained model is developed in order to eliminate internal atomistic degrees of freedom which

are computer time-consuming. The model has no direct connection to any specific PA and the chain is represented as a freely jointed, spherical, and succession of hard beads (physical monomers). Counterions are not explicitly represented. The total number of monomer units is noted N, and the radius of the monomers R_m was set to $l_B/2 = 3.57$ Å, where l_B represents the Bjerrum length. Therefore, to avoid the counterion condensation regime[46] and ensure that interactions may be treated at the Debye–Hückel level, the Manning parameter ξ was imposed equal to 1. Two different types of monomers are taken into account: monomers A and monomers B. In this study, the number of A monomers is equal to the number of B monomers. Only a statistical PA is considered, and the monomer distribution along a linear chain is correlated according to the primary structure $(A_nB_n)_{N/2n}$, where n is the block length. Consequently, the linear PA exhibits two chain ends made of different types of monomers. Each monomer type can either be neutral or carry a charge on its centers. Monomers A are regarded as carboxylic groups in amino acids and have a pK_a^A value fixed to 2.17 in order to simulate the mean acid/base property of such groups. Then, A monomers can be neutral or negatively charged. The pK_a^B value for B monomers is set to 9.53 in order to simulate the mean acid/base property of an amino group in amino acids. Then, monomer B can be positively charged or neutral. For the sake of clarity, Figure 1 summarizes the three characteristic cases and colors codes in the absence of electrostatic interactions between monomers (ideal case).

The fraction of charged monomers of type i (A or B) is noted α_i. In the absence of electrostatic interactions (denoted *ideal conditions*), and according to the solution pH, α_A and α_B are respectively equal to

$$\alpha_A = \frac{K_a^A}{K_a^A + [H^+]} \tag{1}$$

and

$$\alpha_B = \frac{[H^+]}{[H^+] + K_a^B} \tag{2}$$

Titration curves are defined as the variation of α_i as a function of the solution pH and have been proven to be a valuable approach in the understanding of the acid/base properties of weak charged polymers in previous studies.[43,45,47] Titration curves calculated from eqs 1 and 2 are termed as *ideal curves* and are presented in Figure 2a. For the sake of clarity, the titration curves are given and systematically discussed for two different regimes: (i) the low pH regime, when $0 \leq pH \leq \frac{1}{2}(pK_a^A + pK_a^B) = 5.85$ and (ii) the high pH regime, when $5.85 < pH \leq 14$. As shown in Figure 2a, at the isoelectric point pH = 5.85 and both α_A and α_B are equal to one.

In the low pH regime monomers B are fully protonated and exhibit positive charges whereas the ionization degree of monomers A (negative charges) is rapidly decreasing with pH. On the other hand, in the high pH regime, B monomers are deprotonated (neutral), whereas A monomers exhibit negative charges (deprotonated). In this case both titration curves are symmetric with regards to the pH value corresponding to the isoelectric point at pH = 5.85.

The nanoparticle is represented as an impenetrable and solvent excluded sphere with a constant radius $R_{np} = 35.7$ Å. A positive charge Q is assumed to be concentrated into a point located on its center. In such conditions, the central point charge
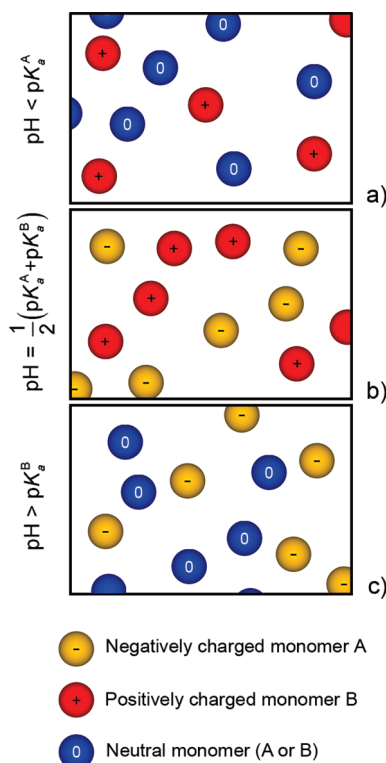

Figure 1. Schematic representation of the monomer unit charge values at different pH conditions: (a) when pH < pK_a^A, only B monomers are (positively) charged (red spheres); (b) when pH is close to (pK_a^A + pK_a^B)/2, both monomer types are charged; (c) when pH > pK_a^B, only A monomers are (negatively) charged (yellow spheres). Both noncharged monomers A or B are represented by dark blue spheres.

Q mimics a constant and homogeneous surface charge density σ. It is imposed that surface charge density do not vary with pH and (arbitrarily) considered that the first adsorption layer thickness is equal to 1.5 monomer diameter (10.71 Å). Surface charge inversion or *overcharging*, which has attracted significant attention,[48,49] is also discussed. In this paper, overcharging occurs at the NP surface when the number of charged monomers A in the first layer, A_{first}^-, is strictly larger than the NP positive charge Q:

$$A_{first}^- > Q \tag{3}$$

It should be noted that monomer and nanoparticle sizes are constant. Their sizes appear different from one snapshot to another due to the limited available space to represent extended conformations. Hard-sphere repulsions between the different units (monomers and NP) are described using hard-core interactions. Electrostatic interactions are treated on the Debye–Hückel level.[50] The solvent is treated as a dielectric continuum with permittivity $\varepsilon_r = 78.5$ equal to that of water at $T = 298$ K. The long-range repulsive electrostatic potential along the distance r_{ij} between charged units i and j is described according to

$$u_{el}(r_{ij}) = \frac{z_i z_j e^2}{4\pi\varepsilon_r\varepsilon_0 r_{ij} k_B T} \frac{\exp[-\kappa(r_{ij} - (R_i + R_j))]}{(1 + \kappa R_i)(1 + \kappa R_j)} \tag{4}$$

where e is the elementary charge ($e = 1.6 \times 10^{-19}$ C), ε_0 the permittivity of the vacuum ($\varepsilon_0 = 8.85 \times 10^{-12}$ C V^{-1} m^{-1}), and z_i the amount of charge on the units i. R_i represents the radius of
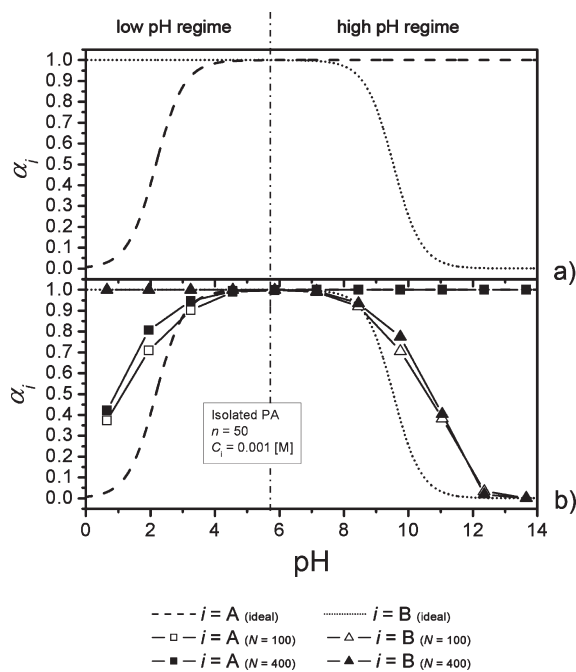
Figure 2. (a) Ideal titration curves in absence of electrostatic interactions between the monomers. (b) Titration curves of an isolated polyampholyte with two different number N of monomers ($N = 100$ and 400) and a block length $n = 50$. Titration curves indicate that the electrostatic attractive intramolecular interactions within the chain significantly modify the acid/base properties of the PA chain.

the spherical units i. The overall effect of free ions in solution is described via the dependence of the inverse Debye screening length κ^2 (m^{-2}) on the ionic concentration as

$$\kappa^2 = \frac{1000e^2 N_A}{\varepsilon_0 \varepsilon_r k_B T} \sum_i z_i^2 C_i \tag{5}$$

where N_A represents the Avogadro number ($N_A = 6.022 \times 10^{23}$ mol^{-1}) and C_i the ionic concentration (mol L^{-1}).

PA titration curves are calculated using Metropolis Monte Carlo simulations in a grand canonical ensemble. Simulations follow two steps: (i) Chain conformations are sampled to obtain a low-energy conformation. An initial set of particles (monomers from the PA and NP positions is randomly chosen, with excluded volume conditions) in a large three-dimensional spherical box having a radius equal to $4NR_m$. To generate new conformations, the monomer positions are randomly modified by random movements (end-bond, kink-jump, and pivot). (ii) After 10 000 Monte Carlo steps, monomers are chosen randomly in the limit of $N/4$ monomers, and their charge states are modified. The energy variation associated with the probability for accepting a new charge state is the sum of the change in the electrostatic interaction ΔE_c and a term that corresponds to the change in free energy of the intrinsic association reaction of a monomer:

$$\Delta E_{tot} = \Delta E_c \pm (\chi(pH - pK_a^i) \ln(10)) \tag{6}$$

The $\pm$ sign is changed depending on whether a protonation ($+$) or deprotonation ($-$) is attempted. The constant χ is equal to $+1$ or -1 when a monomer A or B is respectively considered. It should be noted that pH is an imposed input parameter and the

degree of ionization α_i is calculated by averaging the ionization over a type of monomer i at a given pH.

The Monte Carlo simulations consist of an equilibration period followed by a production period. During the first period, the system is not at equilibrium but converges toward this state. During the production period, the system fluctuates around an equilibrated position. The expectation value of any observable is its average value; i.e., the sum divided by the number of iterations during the production period and a large number of iterations to reach equilibrium has to be considered. Convergence is well reached if there is no drift in the evolution of the observable properties according to the number of steps. In this paper, 1 million steps were typically necessary to reach such conditions.

3. RESULTS AND DISCUSSION

3.1. Isolated Weak Polyampholytes Titration Curves. The acid/base properties of charged polymers largely depend on their conformations,[43,47] and typically, the conformation of a charged polymer in the presence of a nanoparticle depends on three parameters: (i) the intramolecular interactions along the chain, (ii) the intermolecular interactions with the NP, and (iii) the total persistence length of the polymer chain which is related to its intrinsic and electrostatic persistence lengths. To consider first the PA intramolecular electrostatic interaction effects, we carried out simulations with flexible and isolated polyampholytes at an ionic concentration C_i equal to 0.001 mol L^{-1} and a block length equal to $n = 50$. Two monomer numbers N were considered with $N = 100$ and 400, hence corresponding to the cases of diblock and octablock PAs. Simulations with $N = 500$ and 600 were also performed, and an asymptotic behavior was observed when $N \geq$ 400. According to this observation and to handle with reasonable computer time, the chain maximum size was set to $N = 400$.

Titration curves of isolated PAs are then presented in Figure 2b. In the low pH regime, the degree of ionization of monomers B, α_B, is found equal to 1.00 (protonated) and the degree of ionization of monomers A, α_A, significantly larger than in the ideal case. Because of the presence of positively charged B monomers and chain connectivity effects, monomers A deprotonation is thus promoted at low pH, and dense conformations are achieved to optimize the attractive PA intramolecular interactions and chain electrostatic charge coupling. A similar situation is obtained in the high pH regime with regards to the α_B variations which increases significantly in comparison to the ideal case. In this regime, ionization of monomers B is thus promoted to maintain the electrostatic coupling with the negatively charged monomers A. When the chain length N influence is considered, α_i are shown to increase with the increase of N and thus the total number of blocks on the PA which are increasing the total possible conformations and monomers arrangements of the PA chain.

3.2. Complex Formation Influence on the Polyampholyte Titration Curves. To get an insight into the PA acid/base changes due to complex formation, the NP surface charge density and the ionic concentration are respectively fixed to $+100$ mC/ m^2 and 0.001 mol L^{-1}, whereas the block length is set to $n = 50$. Two PA lengths are considered ($N = 100$ and 400), and the corresponding titration curves are presented in Figure 3a. When $N = 100$ (diblock PA), in the low pH regime, the electrostatic interactions resulting from the complexation process between the PA and the positively charged NP clearly promote the ionization of monomers A (creation of negative charges). As a
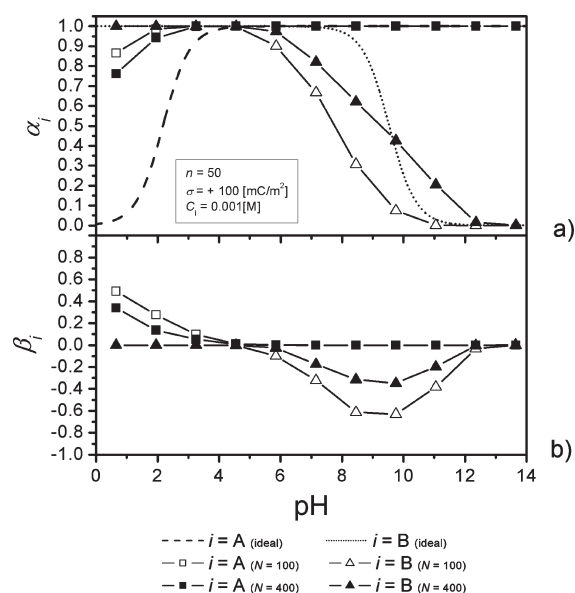
Figure 3. (a) Titration curves of a weak polyampholytes with a block length $n = 50$ and different number N of monomers ($N = 100$ and 400) in the presence of a nanoparticle with a surface charge density $\sigma = +100$ mC m^{-2}. The ionic concentration is set to $C_i = 0.001$ mol L^{-1}. It is shown here that the presence of one nanoparticle results in an asymmetric shape which denotes a complex interplay of the inter- and intramolecular interactions. (b) Variations of β_i as a function of pH for different N allowing comparisons between the isolated and nanoparticle/polyampholyte case. When β_i is positive, the presence of the nanoparticle promotes monomer charges, whereas when β_i is negative, it penalizes their creation in comparison with the isolated case. The presence here of the positively charged nanoparticle promotes the creation of negative charges and reduces the amount of positive charges on the PA chain.

Table 1. Equilibrated Conformations of a Weak Polyampholyte Diblock Forming a Complex with a Positively Charged Nanoparticle with $\sigma = +100$ mC/m^2 [a]
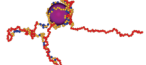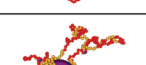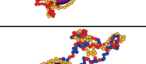

[a] Monomer and nanoparticle sizes are constant. Their sizes appear different from one cell to another due to the lack of available space for representing the extended conformations. The number of monomers is $N = 100$, and the block length is $n = 50$. The ionic concentration is fixed to $C_i = 0.001$ M. Yellow monomers: negatively charged A monomers. Red monomers: charged B monomers. Blue monomers: noncharged A or B monomers. The positively charged monomers are forming a protruding tail because of the strong electrostatic repulsions with the positively charged nanoparticle.

result, even at low pH values, most of them are negatively charged. It is shown in Table 1, in which snapshots of equilibrated conformations are presented, that the A-block wraps the NP, whereas the charged B-block forms a tail which rises up into the solution and does not return to the NP surface. The B-block conformation is related to the long-range electrostatic repulsive interactions between the positively charged NP and the positively charged B monomers and electrostatic persistence length of the charged block.

In the high pH regime, monomers A are still ionized, whereas monomers B neutralization is significantly promoted here to reduce the repulsive interactions with the NP. As a result, α_B is found smaller than the ideal case at a given pH value. The single tail which was present in the low pH regime (Table 1) is found here to collapse with the increase of pH.

The presence of the positively charged NP largely modifies the acid/base properties of the PA chains, resulting in asymmetric titration curves with regards to the isoelectric point position. To evaluate in a simple way the effective NP effect (i.e., in comparison to the acid–base properties of the isolated PA in solution), the parameter β_i is introduced and defined as

$$\beta_i = \alpha_i^{np} - \alpha_i^{isolated} \tag{7}$$

where α_i^{np} is the fraction of ionized monomers of type i ($i = A$ or B) in the presence of the NP and $\alpha_i^{isolated}$ the fraction of ionized monomers in the absence of the NP at a given pH. When β_i is positive, the presence of the NP globally promotes the creation of

charges on the PA chain and vice versa. The variations of β_i as a function of pH are presented in Figure 3b. It is shown that β_A is positive in the low pH regime but decreases with the increase of pH and reaches a zero value when pH = 5.85, i.e., at the isoelectric point. When $\beta_i = 0$, the mean acid/base properties of the i monomers are not influenced by the NP. On the other hand, when β_i is negative, the NP penalizes the presence of positively charged monomers B. In our case, due to the positively charged NP, β_B is negative when 4.55 < pH < 12.35.

3.3. Chain Length Influence on the Structures of the NP–PA Complexes. Simulations with $N = 400$ (octablock PA) are here under considerations and compared to the results obtained with $N = 100$ (diblock PA). As shown in Table 2, owing to the important contour length of the PA octablock in comparison to the NP size, the direct influence of steric effects, number of blocks, and charge distribution along the chain is observed. Loops and tails composed mainly of appositely charged and neutral monomers are obtained with the PA octablock. The corresponding titration curves are presented in Figure 3a and β_i variations in Figure 3b. The influence of the NP is found to be less important on the large octablock PA in comparison to the small diblock PA. On the one hand, in the low pH regime, for the octablock only three A blocks (negatively charged) are in the close NP vicinity, whereas all the A monomers of the diblock PA are adsorbed at the NP surface. As a result, in the low pH regime, α_A decreases with the increase of N, and the influence of the NP on the β_i parameter is less important for the octablock PA (Figure 3b). On the other hand, in the high pH regime, ionization

Table 2. Equilibrated Conformations of a Weak Polyampholyte Forming a Complex with a Positively Charged Nanoparticle with $\sigma = +100$ mC/m^2 ^{a}

		Chain properties
		$N = 400$; $n = 50$
pH	0.65	
	3.25	
	5.85	
	8.45	
	11.05	

^{a} The number of monomers is $N = 400$, and the block length is $n = 50$. The ionic concentration is fixed to $C_i = 0.001$ M. The positively charged B monomer blocks are forming extended loops at the NP surface in which charge coupling between the positively and negatively charged is observed. Yellow monomers: negatively charged A monomers. Red monomers: charged B monomers. Blue monomers: noncharged A or B monomers.

a)

b)

— ■ — Monomers A
— ▲ — Monomers B

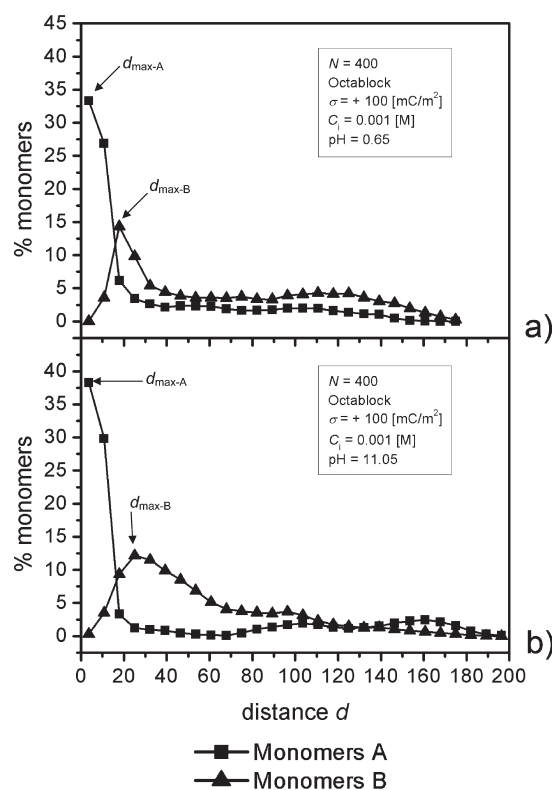**Figure 4.** Radial monomer distributions with $N = 400$ and $n = 50$ in the presence of a nanoparticle with $\sigma = +100$ mC m^{-2} with $C_i = 0.001$ mol L^{-1}. (a) pH = 0.65; 120 A monomers are situated in the nanoparticle first adsorption layer and charge inversion is observed (negative). This promotes the adsorption of a second layer made of positively charged B monomers. The maximum radial distribution of monomers B is found very close to the first adsorption layer ($d_{max-B} = 17.85$ Å). (b) pH = 11.05; the maximum radial distribution of monomers B is situated at a larger distance of the nanoparticle ($d_{max-B} = 24.99$ Å) since B monomers are neutral in this pH condition and do no interact directly with the negatively charged A monomers.

of B monomers is more important for the octablock PA. Additionally, the titration curve when $N = 400$ present two different parts with regards to the ideal curve. When 5.85 < pH < 9.75, the neutralization of monomers B decreases the repulsive electrostatic interactions with the NP. When pH $\geq$ 9.75, neutralization of B monomers is found unfavorable in comparison to the ideal case, owing to the need to maintain the electrostatic coupling with the negatively charged A blocks in the loops at a distance from the NP surface.

To get an insight into the distribution of the PA octablock monomers around the NP surface, the average monomer radial distribution was calculated. In the low pH regime, when pH = 0.65 (Figure 4a), about 59% of the negatively charged A monomers (i.e., $A_{first}^- = 118$) are situated in the NP first layer, and as a result, NP overcharging is observed. It is also found that the maximum density of monomers B is located at a distance $d = 17.85$ Å from the surface, just after the A monomer peak, hence suggesting the formation of a multilayer structure composed of negatively charged monomers A and positively charged B monomers.

3.4. Ionic Concentration Effect. To get an insight into the effects of charge screening, simulations are carried out at different ionic concentrations ($C_i = 0.1$, 0.01, and 0.001 mol L^{-1}): The chain length is set to $N = 400$, block length $n = 50$, and NP surface charge density to $\sigma = +100$ mC m^{-2}. As shown in Figure 5a, titration curves are found highly dependent on the ionic concentration. In the low pH regime, at a given pH value, α_A decreases with the increase of the ionic concentration which attenuates the electrostatic interactions not only between the PA

charged monomers but also between the PA and the charged NP. Consequently, when $C_i = 0.1$ mol L^{-1}, the resulting titration curve is close to the ideal case.

In the high pH regime, the situation is more complex and depends on the pH value. Indeed, when 5.85 < pH < 9.75, α_B increases with the increase of the ionic concentration due to the decrease of repulsive electrostatic interactions between the positively charged monomers B and the positive NP. When pH > 9.75 and $C_i = 0.1$ and 0.01 mol L^{-1}, charge coupling between the negative and positive monomers at the surface of the NP promotes the formation of positive charges in particular at low ionic strength. When β_A is considered in Figure 5b, at a given pH in the low pH regime, β_A increases with the decrease of C_i, whereas β_B is found negative in the high pH regime. It should be noted that β_A are always positive excepted at pH = 0.65 and $C_i = 0.1$ mol L^{-1} where $\beta_A = 0$. Such a behavior is due to the desorption of the PA from the NP surface. To account for chain desorption, a pH$_{critic}$ value was defined, corresponding to the pH value at which desorption is observed; i.e., when pH $\leq$ pH$_{critic}$, no complex is observed. It is found here that, when $C_i = 0.1$ mol L^{-1}, pH$_{critic} = 1.85$.

3.5. Nanoparticle Surface Charge Density Influence. To vary the strength of the intermolecular interactions between the
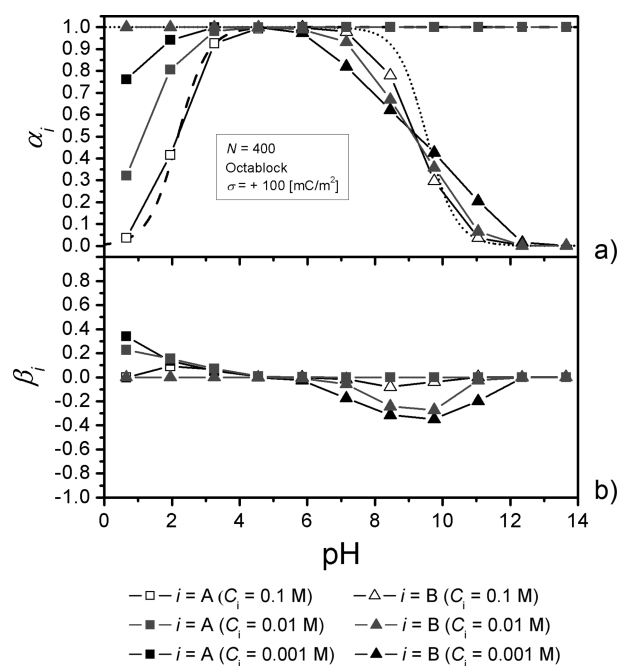
Figure 5. (a) Titration curves of a weak polyampholyte with $N = 400$ and $n = 50$, in the presence of a nanoparticle with a surface charge density $\sigma = +100$ mC m^{-2}. Three different ionic concentrations are considered: $C_i = 0.001$, 0.01, and 0.1 mol L^{-1}. β_i variations as a function of pH and ionic concentrations are presented in (b). It is shown here that the charge screening reduces the impact of the complexation process as well as the intramolecular interactions within the PA on the acid/base properties of the PA.

NP and the PA, the NP surface charge density σ is now adjusted. Three different σ values are compared ($\sigma = +10$, $+50$, and $+100$ mC m^{-2}). The ionic concentration is fixed to $C_i = 0.001$ mol L^{-1} and the PA length to $N = 400$, and equilibrated conformations are presented in Table 3. As shown in Figure 6a, in the low pH regime, monomers A deprotonation is promoted with the increase of σ, whereas in the high pH regime, monomers B protonation is found to increase with the decreases of the NP surface charge density.

The case of $\sigma = +10$ mC m^{-2} is first considered to account for a weakly charged NP. When pH = 0.65, all B monomers are charged, whereas a small fractions of A monomers are negatively charged. As shown in Table 3, no complex is formed, and the charged blocks adopt a stretched conformation because of the repulsions between positively charged blocks. When pH = 5.85 (isoelectric point), both A and B monomers are charged. The electrostatic interactions create correlations between monomers of opposite signs, and as a result, the chain size is minimum, in good agreement with Higgs and Joanny.[51] When pH = 11.05, A monomers are negatively charged whereas most of the monomers B are neutral. Thus, complexation with NP occurs with only one adsorbed A block. In such conditions, pH$_{\text{critic}}$ is high and equal to 9.25.

At intermediate NP surface charge ($\sigma = +50$ mC/m^2) and when pH = 0.65, no complex is formed and the chain adopt a stretched conformation. pH$_{\text{critic}}$ is found equal to 1.85, and complex formation is observed systematically above this value. In Table 3, a particular conformation can be observed when pH = 5.85 since dense multilayers are achieved at the NP surface. This conformation is typically reached at intermediate σ values. The

Table 3. Equilibrated Conformations of a Weak Polyampholyte with $N = 400$ and $n = 50$ Forming a Complex with a Positively Charged Nanoparticle with Different Value of Surface Charge Densities σ^a

^{a} The ionic concentration is fixed to $C_i = 0.001$ M. Yellow monomers: negatively charged A monomers. Red monomers: charged B monomers. Blue monomers: noncharged A or B monomers. The importance and effect of the PA intramolecular interactions (charge coupling between A and B monomers) as well as the final PA conformation at the surface of the nanoparticle are largely controlled by the surface charge density of the nanoparticle. Monomer and nanoparticle sizes are constant. Their sizes appear different from one cell to another due to the lack of available space for representing the extended conformations.

average monomer radial distribution is calculated and given in Figure 7. It is found that $A^-_{\text{first}} = 127$, thus leading to a strong NP overcharging. This overcharging contributes to the formation of multilayers since B monomers radial distribution starts to increase with the increase of d and reaches a maximum value at 17.65 Å, i.e., just after the peak corresponding to the A monomers distribution in the first adsorption layer. By further increasing d, a second peak in the monomers A radial distribution is found at 74.97 Å and then followed by a second peak at 82.11 Å due to B monomers radial distribution. When pH = 11.05, a large tail made of neutral monomers B rising to the solution is achieved. This tail is also made of charged monomers A because their full confinement at the NP surface is not possible owing to the absence of positively charged B monomers.

When $\sigma = +100$ mC/m^2, as shown in Table 3, the presence of a highly charged NP is significantly changing the adsorbed PA conformation. Indeed, large protruding loops are achieved which result from the strong electrostatic repulsions between the positively charged monomers blocks and the NP.

3.6. Polyampholyte Block Length Influence. In this section the block length is decreased to $n = 13$ so as to consider smaller blocks. The PA chain length is fixed to $N = 104$ in order to consider a small PA octablock. The NP surface charge density and the ionic concentration are respectively fixed to $\sigma = +100$ mC m^{-2} and $C_i = 0.001$ mol L^{-1}. The influences of n on
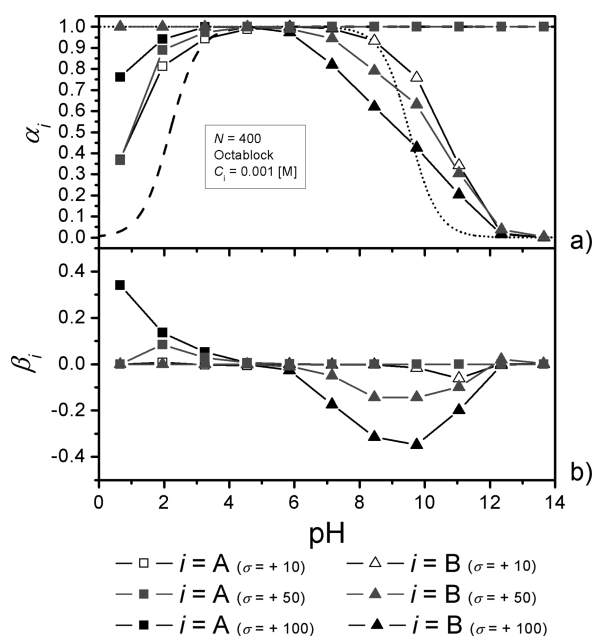
Figure 6. (a) Titration curves of a weak octacblock polyampholyte with $N = 400$, $n = 50$, and $C_i = 0.001$ mol L^{-1}. The nanoparticle surface charge is adjusted to $\sigma = +10$, 50, and 100 mC m^{-2}. β_i variations as a function of pH are presented in (b). The PA acid/base property changes are proportional to the surface charge of the NP. The highly charged nanoparticle has a strong impact on the charging and decharging behavior of the PA in comparison to the ideal case.
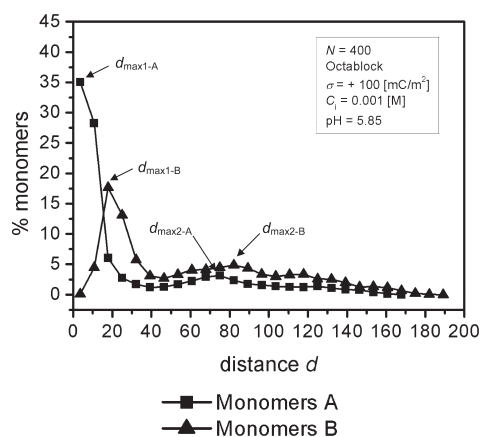

Figure 7. Radial monomer distributions of an octablock polyampholyte with $N = 400$ and $n = 50$ adsorbed at the surface of a nanoparticle with $\sigma = +50$ mC m^{-2}, $C_i = 0.001$ mol L^{-1} at pH = 5.85. 126 charged A monomers are situated in the nanoparticle first layer and result in a strong charge inversion. Multilayers made of successive monomers A and B are then observed.

complexation and acid/base properties are compared with the previous diblock PA results ($N = 100$ and $n = 50$). Snapshots of equilibrated conformations of complexes are presented in Table 4 and titration curves in Figure 8. As shown in Table 4, in the low pH regime, multiple trains between blocks made of A monomers and the NP are achieved. Such multiloop conformations are similar to the rosette structures[43,52] obtained with a semiflexible polyelectrolyte and an oppositely charged macroion and are usually termed *electrostatic rosette* conformation. Here the intermolecular interactions between the positively and

Table 4. Equilibrated Conformations of a Weak Polyampholyte Forming a Complex with a Positively Charged Nanoparticle with $\sigma = +100$ mC/m^2 [a]

[a] The number of monomers is $N = 104$, and the block length is $n = 13$. The ionic concentration is fixed to $C_i = 0.001$ M. The presence of blocks with sizes close to the NP diameter result in the formation of electrostatic rosettes at low pH.
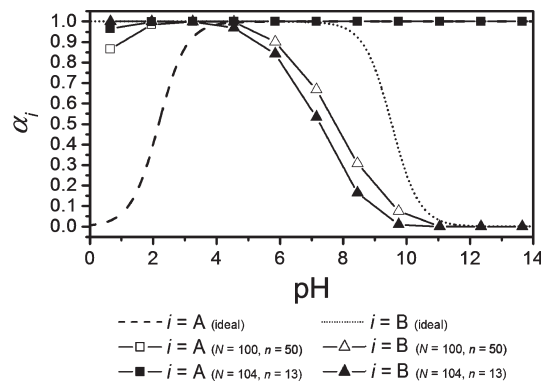

Figure 8. Titration curves of a weak polyampholyte in presence of a nanoparticle with $\sigma = +100$ mC m^{-2}. Two chains are considered with different block and chain lengths: (i) $n = 50$ and $N = 100$ and (ii) $n = 13$ and $N = 104$. The ionic concentration is set to $C_i = 0.001$ mol L^{-1}. Small block lengths promote here the creation of negative charges at low pH as well as the decrease of the positive charges along the PA chain.

negatively charged monomers of the PA are not playing a significant role in the final complex structure. In Figure 8, it is shown that the titration curves are dependent on the block length. At low pH, the presence of small blocks permits to optimize the contacts between the A block and the oppositely charged NP surface. In the high pH regime α_B decreases with the decrease of block length because of the numbers of relatively small confined loops made of charged B monomers which, from an electrostatic point of view, strongly interact with the NP. With large blocks, the positively charged B monomers are able to escape from the NP surface and are less affected. Owing to the importance of the knowledge of PA adsorption/desorption limits for a practical
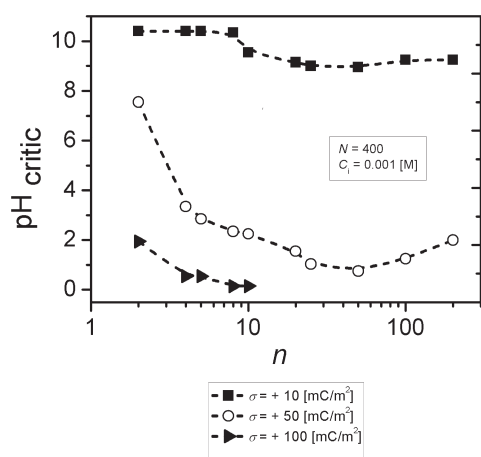
Figure 9. Variation of the pH_{critic} as a function of block length n for different nanoparticle charge densities ($\sigma = +10$, 50, or 100 mC m^{-2}). pH_{critic} is defined as the pH value at which desorption is observed when $pH \leq pH_{critic}$. Increasing the size of the blocks results in a decrease of the pH_{critic} value and thus increases the complex formation domain.

and rational use of PAs in flocculation processes and nanoparticle stabilization, the influence of the block length n on adsorption/desorption limit is also investigated here. Complementary simulations with different values of n are carried out with $N = 400$ and $C_i = 0.001$ mol L^{-1}. Three different σ values are also considered ($\sigma = +10$, $+50$, and $+100$ mC m^{-2}) to achieve a full picture. The variation of pH_{critic} as a function of the primary structure (n value) is presented in Figure 9. Stable complexes are obtained above the pH_{critic} curves. Complex formation stability domain is found to depend not only on the pH and NP surface density but also on the block sizes. Small PA block sizes clearly penalizes the formation of stable complexes as well as the presence of large blocks. As a result, the best conditions for complex formation are here obtained when the A block length is of the order of the NP diameter.

4. CONCLUSIONS

In this paper the electrostatic driven complexation process between a polyampholyte chain and a charged nanoparticle is investigated by simulations. The subtle interplay between the attractive and repulsive, intermolecular and intramolecular, electrostatic interactions as well as the impact of the pH, surface charge of the nanoparticle, and ionic strength are presented via the analysis of titration curves, radial distribution functions, and equilibrated conformation pictures. For the first time, using computer simulations, the analysis of the titration curves clearly demonstrates that the presence of a charged nanoparticle largely modifies the acid/base properties of a polyampholyte. On the one hand, in the presence of a positively charged NP, the latter promotes the formation of negatively charged monomers and, on the other hand, penalizes the formation of positive monomer charges. Depending on the NP charge surface, different PA conformations are achieved at the NP surface ranging from condensed conformations (at intermediate surface charge) to electrostatic rosettes (at high surface charge). At low NP surface charge density, the adsorption of the PA at the NP surface is difficult to achieve. Also the PA geometry is shown to play an important role not only on acid base properties but also on the PA conformation at the NP surface. Diblock PAs lead to the

adsorption of the oppositely charged PA, whereas the second block having the same charge than the NP is forming a protruding tail in the solution. It is also important to note that the electrostatic charge coupling between the PA monomers also affects to a large extent the final conformation of the complexes in particular at pH close to the PA isoelectric point. The formation of multiplayer structure is achieved in particular conditions of pH, NP surface charge density, and overcharging as well as PA structure.

From a general point of view our simulations allow to predict directly the protonation state of polyampholytes, relating the charge state to the local electrostatic potential. From a perspective point of view, the modeling of (nano)particles with charge anisotropy would permit to consider the relative affinities of some polyelectrolytes for target proteins and charge recognition via charge complementarities, hence leading to the optimized design of protein-specific polymer systems and selective surfaces which have considerable values in the biophysics community.

■ AUTHOR INFORMATION

Corresponding Author
*E-mail: serge.ulrich@gmail.com.

■ ACKNOWLEDGMENT

■ REFERENCES

(1) Stuart, M.; Kleijn, J. *Surfactant Sci. Ser.* **2001**, *99*, 281–304.
(2) Tribet, C. *Surfactant Sci. Ser.* **2001**, *99*, 687–741.
(3) Cooper, C.; Dubin, P.; Kayitmazer, A.; Turksen, S. *Curr. Opin. Colloid Interface Sci.* **2005**, *10*, 52–78.
(4) Ciferri, A.; Kudaibergenov, S. *Macromol. Rapid Commun.* **2007**, *28*, 1953–1968.
(5) Kudaibergenov, S.; Ciferri, A. *Macromol. Rapid Commun.* **2007**, *28*, 1969–1986.
(6) Dobrynin, A. *Curr. Opin. Colloid Interface Sci.* **2008**, *13*, 376–388.
(7) Ullner, M. *DNA Interact. Polym. Surfactants* **2008**, 1–39.
(8) Messina, R. *J. Phys.: Condens. Matter* **2009**, *21*, 113102.
(9) Dobrynin, A.; Rubinstein, M. *Prog. Polym. Sci.* **2005**, *30*, 1049–1118.
(10) Decher, G. *Science* **1997**, *277*, 1232–1237.
(11) Berret, J.; Schonbeck, N.; Gazeau, F.; El Kharrat, D.; Sandre, O.; Vacher, A.; Airiau, M. *J. Am. Chem. Soc.* **2006**, *128*, 1755–1761.
(12) Alfrey, T.; Fuoss, R.; Morawetz, H.; Pinner, H. *J. Am. Chem. Soc.* **1952**, *74*, 438–441.
(13) Alfrey, T.; Morawetz, H. *J. Am. Chem. Soc.* **1952**, *74*, 436–438.
(14) Xia, J.; Dubin, P.; Kim, Y.; Muhoberac, B.; Klimkowski, V. *J. Phys. Chem.* **1993**, *97*, 4528–4534.
(15) Dubin, P.; Gao, J.; Mattison, K. *Sep. Purif. Methods* **1994**, *23*, 1–16.
(16) Xia, J.; Dubin, P. *Macromol. Complexes Chem. Biol.* **1994**, 247–271.
(17) Bowman, W.; Rubinstein, M.; Tan, J. *Macromolecules* **1997**, *30*, 3262–3270.
(18) Porcar, I.; Gareil, P.; Tribet, C. *J. Phys. Chem. B* **1998**, *102*, 7906–7909.
(19) Leal Denis, M.; Carballo, R.; Spiaggi, A.; Dabas, P.; Campo Dall' Orto, V.; Martinez, J.; Buldain, G. *React. Funct. Polym.* **2008**, *68*, 169–181.
(20) Dautzenberg, H.; Jaeger, W.; Kötz, J.; Philipp, B.; Seidel, C.; Stscherbina, D. *Polyelectrolytes: Formation, Characterization and Application*; Hanser: Munich, 1994.

(21) Mahltig, B.; Cheval, N.; Gohy, J.; Fahmi, A. *J. Polym. Res.* **2010**, *17*, 579–588.

(22) Kamiyama, Y.; Israelachvili, J. *Macromolecules* **1992**, *25*, 5081–5088.

(23) Ozon, F.; Di Meglio, J.; Joanny, J. *Eur. Phys. J. E* **2002**, *8*, 321–330.

(24) Neyret, S.; Ouali, L.; Candau, F.; Pefferkorn, E. *J. Colloid Interface Sci.* **1995**, *176*, 86–94.

(25) Tran, Y.; Perrin, P.; Deroo, S.; Lafuma, F. *Langmuir* **2006**, *22*, 7543–7551.

(26) Dobrynin, A.; Rubinstein, M.; Joanny, J. *Macromolecules* **1997**, *30*, 4332–4341.

(27) Zhulina, E.; Dobrynin, A.; Rubinstein, M. *Eur. Phys. J. E* **2001**, *5*, 41–49.

(28) Netz, R.; Joanny, J. *Macromolecules* **1998**, *31*, 5123–5141.

(29) Dobrynin, A.; Obukhov, S.; Rubinstein, M. *Macromolecules* **1999**, *32*, 5689–5700.

(30) Dobrynin, A. *Phys. Rev. E* **2001**, *63*, 051802/1–051802/5.

(31) Dobrynin, A.; Zhulina, E.; Rubinstein, M. *Macromolecules* **2001**, *34*, 627–639.

(32) de Vries, R.; Weinbreck, F.; de Kruif, C. *J. Chem. Phys.* **2003**, *118*, 4649–4659.

(33) Weinbreck, F.; de Vries, R.; Schrooyen, P.; de Kruif, C. G. *Biomacromolecules* **2003**, *4*, 293–303.

(34) Feng, J.; Ruckenstein, E. *Polymer* **2003**, *44*, 3141–3150.

(35) Khan, M.; Aakesson, T.; Joensson, B. *Macromolecules* **2001**, *34*, 4216–4221.

(36) Messina, R. *Eur. Phys. J. E* **2007**, *22*, 325–333.

(37) Jeon, J.; Dobrynin, A. V. *J. Phys. Chem. B* **2006**, *110*, 24652–24665.

(38) Yoshihara, C.; Shew, C.; Ito, T.; Koyama, Y. *Biophys. J.* **2010**, *98*, 1257–1266.

(39) Akinchina, A.; Shusharina, N.; Linse, P. *Langmuir* **2004**, *20*, 10351–10360.

(40) Akinchina, A.; Linse, P. *Langmuir* **2007**, *23*, 1465–1472.

(41) Linse, P. *J. Chem. Phys.* **2007**, *126*, 114903/1–114903/13.

(42) Baratlo, M.; Fazli, H. *Phys. Rev. E* **2010**, *81*, 011801.

(43) Ulrich, S.; Laguecir, A.; Stoll, S. *Macromolecules* **2005**, *38*, 8939–8949.

(44) Ulrich, S.; Seijo, M.; Laguecir, A.; Stoll, S. *J. Phys. Chem. B* **2006**, *110*, 20954–20964.

(45) Ulrich, S.; Seijo, M.; Stoll, S. *J. Phys. Chem. B* **2007**, *111*, 8459–8467.

(46) Manning, G. *J. Chem. Phys.* **1969**, *51*, 924–933.

(47) Ulrich, S.; Seijo, M.; Stoll, S. *Curr. Opin. Colloid Interface Sci.* **2006**, *11*, 268–272.

(48) Wang, Y.; Kimura, K.; Huang, Q.; Dubin, P. L.; Jaeger, W. *Macromolecules* **1999**, *32*, 7128–7134.

(49) Martin-Molina, A.; Quesada-Perez, M.; Galisteo-Gonzalez, F.; Hidalgo-Alvarez, R. *Prog. Colloid Polym. Sci.* **2004**, *123*, 114–118.

(50) Verwey, E. J. W.; Overbeek, J. T. G. *Theory of the Stability of Lyophobic Colloids*; Dover Publications: Mineola, NY, 1999.

(51) Higgs, P. G.; Joanny, J. *J. Chem. Phys.* **1991**, *94*, 1543–1554.

(52) Schiessel, H. *Macromolecules* **2003**, *36*, 3424–3431.